Optimizing dielectric polarization for electromagnetic wave attenuation via enhanced Maxwell-Wagner-Sillars effect in hollow carbon microspheres

Baojun Wang[a,1], Hao Wu[a,1], Wenxuan Hou[a], Zhifeng Fang[a], Heqin Liu[a], Fangzhi Huang[b], Shikuo Li[a,], Hui Zhang[a,*]*

[a]*School of Materials Science and Engineering, Anhui University; Key Laboratory of Structure and Functional Regulation of Hybrid Materials (Anhui University), Ministry of Education; Hefei, 230601, PR China*

[b]*School of Chemistry and Chemical Engineering, Anhui University, Hefei, 230601, PR China*

**Corresponding authors: lishikuo@ahu.edu.cn (S. Li), zhhui@ahu.edu.cn (H. Zhang).*

Baojun Wang and Hao Wu contributed equally to this work.

1. Electromagnetic wave absorption performance

The reflection loss values were calculated based on the transmission line theory:[1, 2]

$$Z_{in} = Z_0 \sqrt{\frac{\mu_r}{\varepsilon_r}} \tanh\left(j \frac{2\pi fd}{c} \sqrt{\mu_r \varepsilon_r} \right) \quad (1)$$

$$RL = 20 \log \left| \frac{Z_{in} - Z_0}{Z_{in} + Z_0} \right| \quad (2)$$

where Z_{in} is the normalized input impedance of the absorber, μ_r and ε_r are the relative complex permeability and permittivity, respectively, f is the corresponding frequency and c is the velocity of light in the free space, and d is the thickness of absorbers.

2. Conduction loss and polarization loss

According to Debye theory, the imaginary part (ε") of complex permittivity could be divided into conduction loss (ε''_c) and polarization loss (ε''_p) as following equations:[3, 4]

$$\varepsilon'' = \frac{\omega\tau(\varepsilon_s - \varepsilon_\infty)}{1+\omega^2\tau^2} + \frac{\sigma}{\omega\varepsilon_0} = \varepsilon''_p + \varepsilon''_c \quad (3)$$

$$\varepsilon''_c = \frac{\sigma}{\omega\varepsilon_0} \quad (4)$$

where ω is angular frequency, ε_s is static dielectric constant, τ is polarization relaxation time, ε_0 (8.85×10^{-12} F/m) is the permittivity of free space, ε_∞ is relative permittivity at high frequency and σ is electrical conductivity.

3. Attenuation constant (α)

The α is used to evaluate the comprehensive loss competence of absorbers and is calculated by the following equation:[5, 6]

$$\alpha = \frac{\sqrt{2}\pi f}{c}\sqrt{\left(\mu''\varepsilon'' - \mu'\varepsilon'\right) + \sqrt{\left(\mu''\varepsilon'' - \mu'\varepsilon'\right)^2 + \left(\mu'\varepsilon'' + \mu''\varepsilon'\right)^2}} \quad (5)$$

where μ' and μ'' are the real part and imaginary part of the complex permeability respectively, ε' and ε'' are the real part and imaginary part of the complex permittivity respectively, f is the frequency of the electromagnetic wave and c is the velocity of light in free space.

4. Radar cross section simulation

The radar cross section (RCS) simulation was performed on CST Studio Suite 2019. The measured real part and imaginary part of complex permittivity and complex permeability were input to the simulation software. The model with 180 mm square consists of an upper absorbing layer (2 mm) and bottom perfect electric conductor layer (PEC, 0.5 mm). The model plate was placed on the XOY plane. The scattering direction was determined by θ and φ in spherical coordinates, and the selected field monitor frequency was 15.2 GHz. For a certain scattering source, it is generally accepted that the scattering directions of RCS value (σ) can be determined by theta and phi in spherical coordinates, which can be described as:[7, 8]

$$\sigma\left(dBm^2\right) = 10\log\left[\frac{4\pi S}{\lambda^2}\left|\frac{E_s}{E_i}\right|^2\right] \quad (6)$$

where, S, λ, E_s, and E_i are the area of the simulated plate, the wavelength of the incident electromagnetic wave, the electric field strength of the transmitted and received waves, respectively.

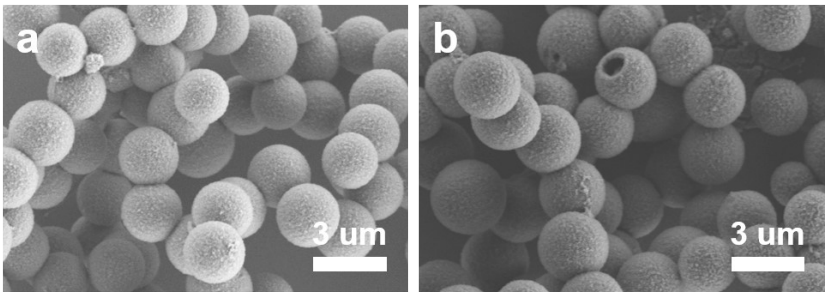

Fig. S1 (a, b) The FE-SEM images of hollow Ni-BTC.

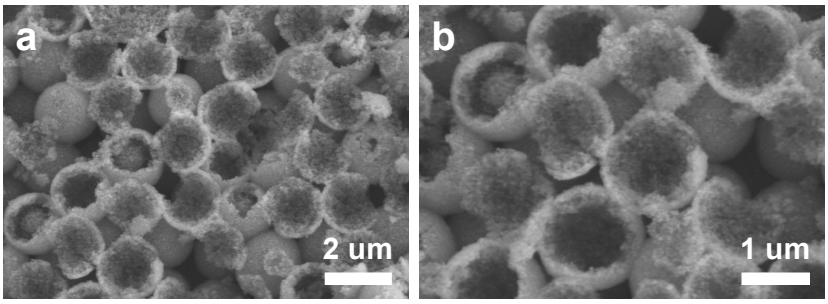

Fig. S2 (a, b) The cross-section of FE-SEM images of hollow Ni/Ni_2P/CNs-2.

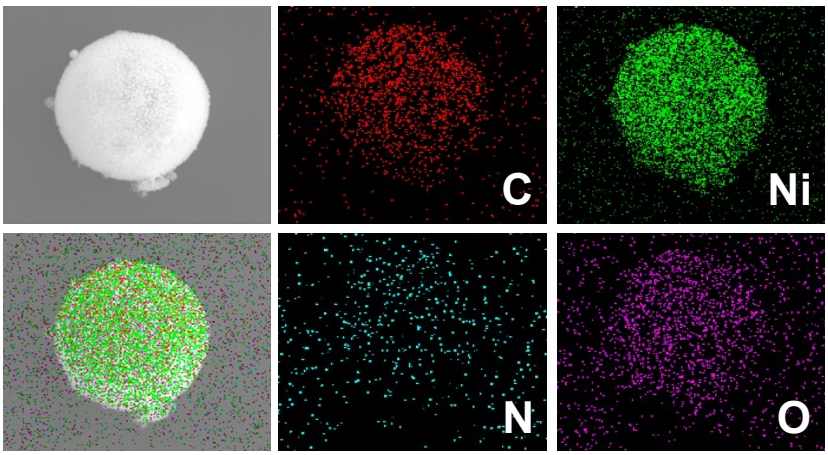

Fig. S3 EDS elemental mapping images of Ni/C.

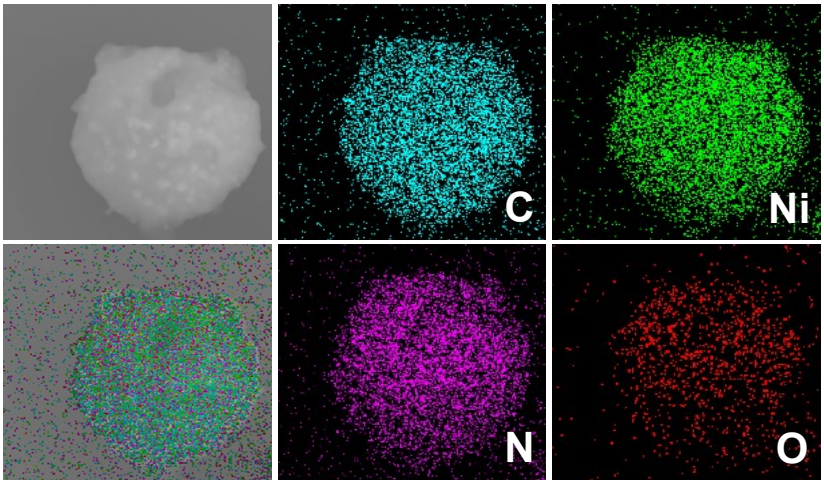

Fig. S4 EDS elemental mapping images of Ni/CNs.

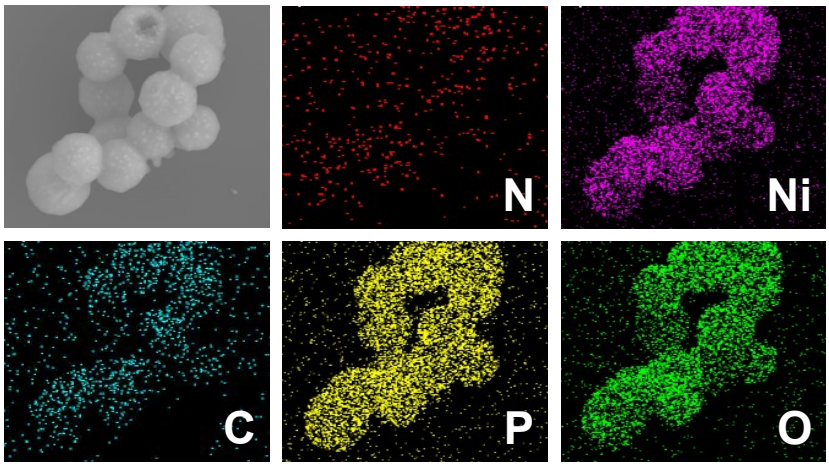

Fig. S5 EDS elemental mapping images of Ni/Ni_2P/CNs-1.

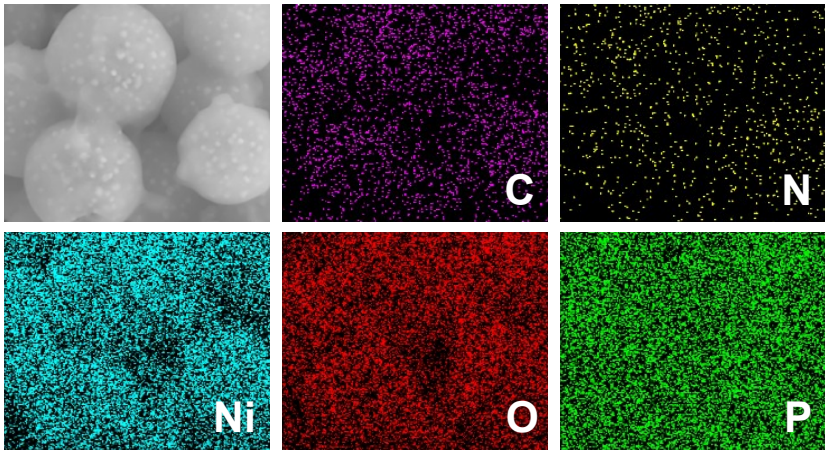

Fig. S6 EDS elemental mapping images of Ni/Ni_2P/CNs-3.

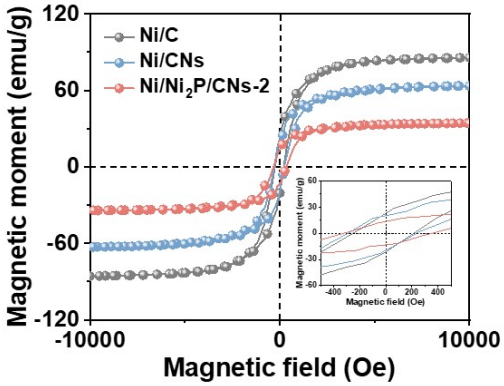

Fig. S7 Magnetic hysteresis loops of Ni/C, Ni/CNs, and Ni/Ni2P/CNs-2.

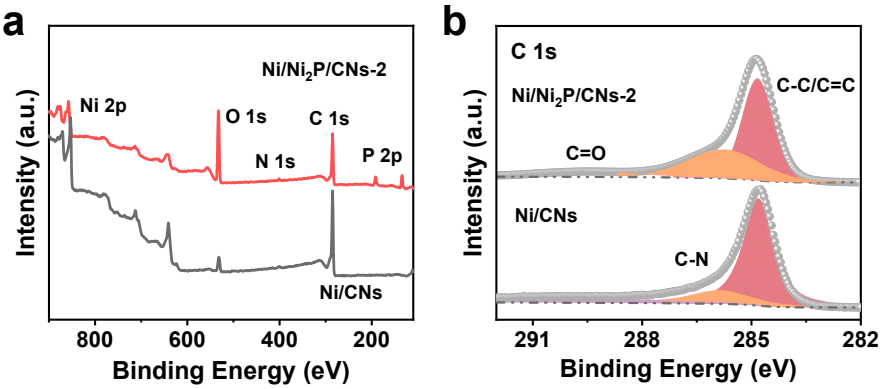

Fig. S8 (a) The XPS spectra and (b) C 1s spectrum of Ni/CNs and Ni/Ni_2P/CNs-2 samples.

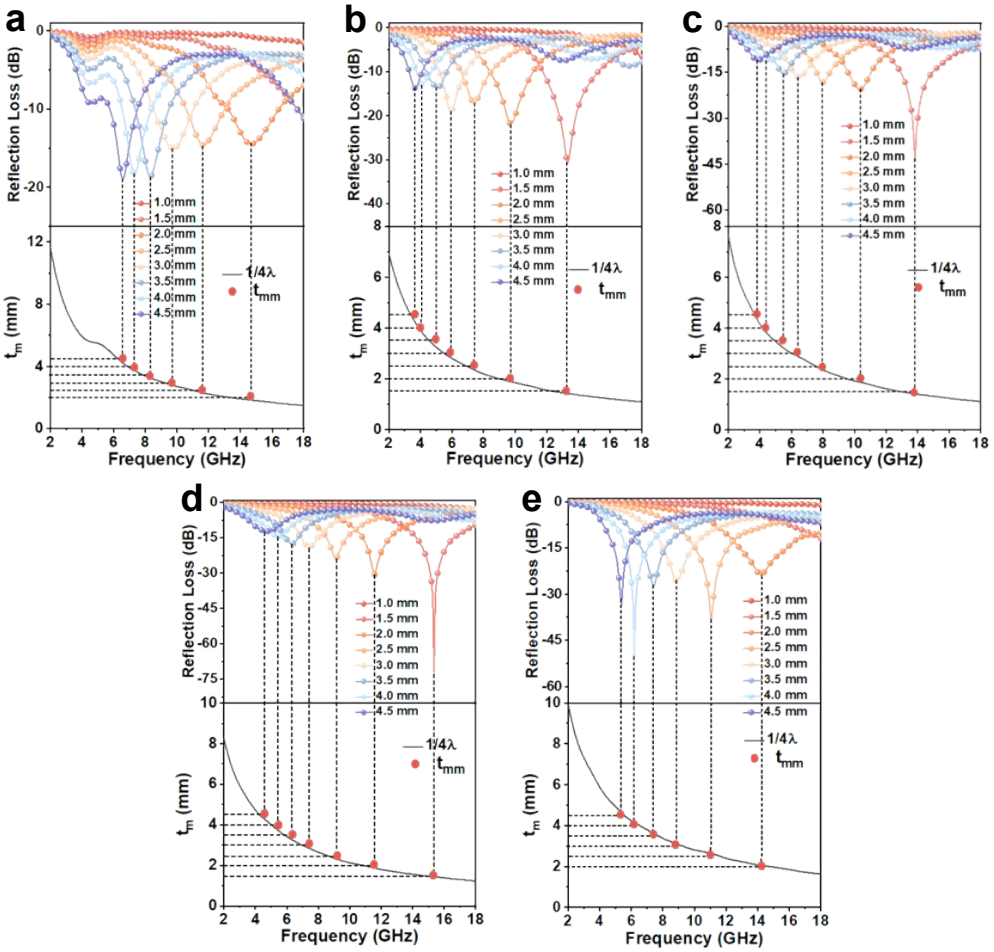

Fig. S9 2D RL values and dependence of matching thickness (t_m) on frequency (f_m) under λ/4 of (a) Ni/C, (b) Ni/CNs, (c) Ni/Ni_2P/CNs-1, (d) Ni/Ni_2P/CNs-2, and (e) Ni/Ni_2P/CNs-3.

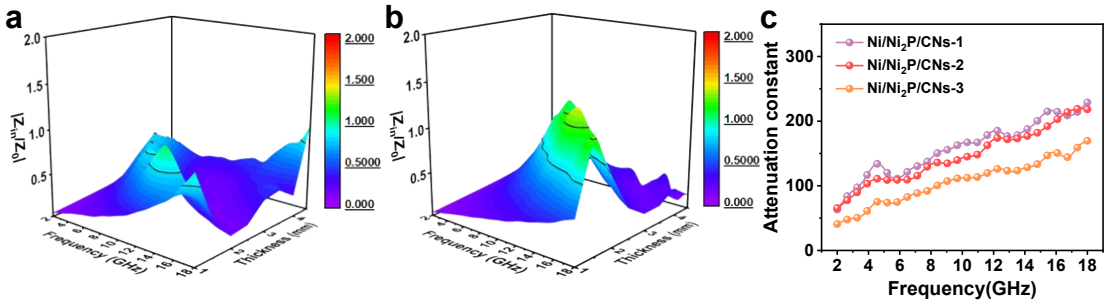

Fig. S10 3D impedance matching (M_z) plots of (a) Ni/Ni_2P/CNs-1 and (b) Ni/Ni_2P/CNs-3. (c) Attenuation constant of Ni/Ni2P/CNs-x.

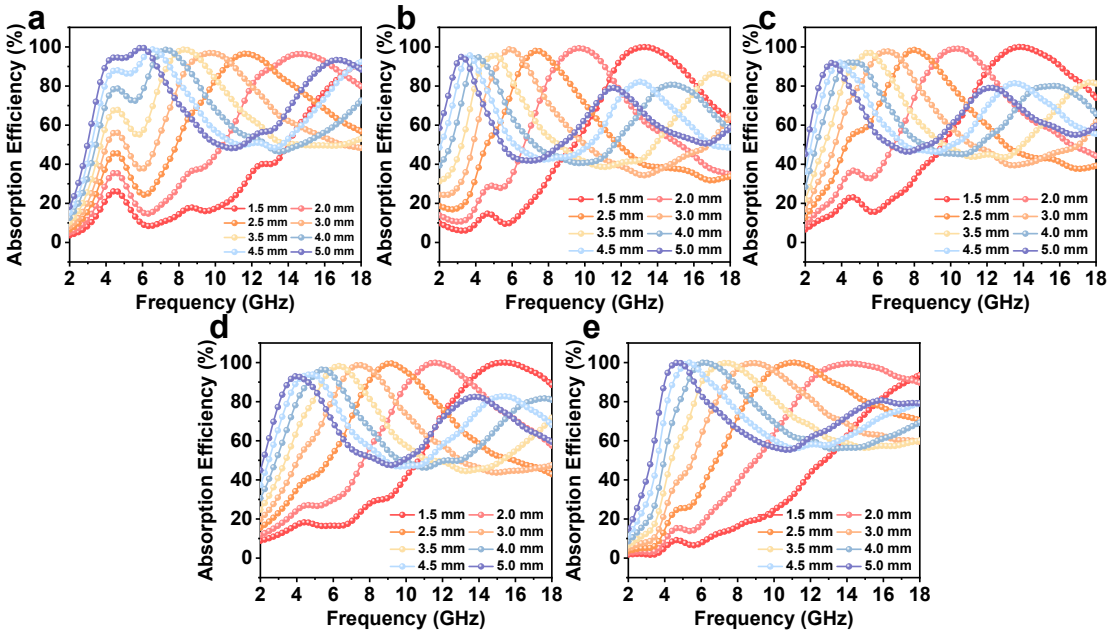

Fig. S11 Absorption efficiency of (a) Ni/C, (b) Ni/CNs, (c) Ni/Ni_2P/CNs-1, (d) Ni/Ni_2P/CNs-2, and (e) Ni/Ni_2P/CNs-3.

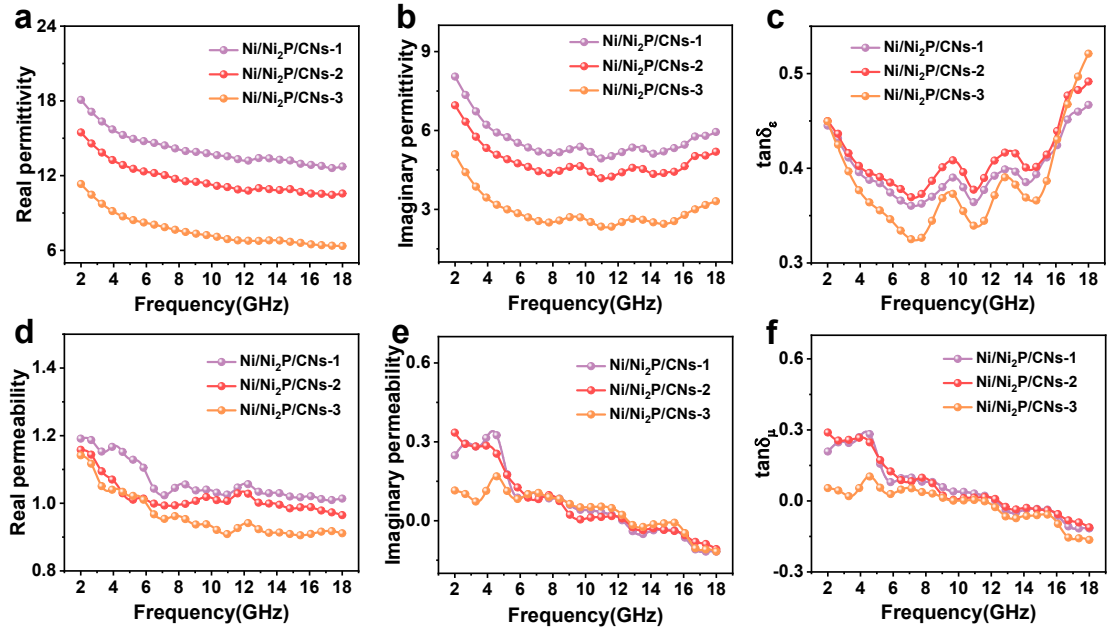

Fig. S12 Electromagnetic parameters of Ni/Ni_2P/CNs-x. (a) Real and (b) imaginary part of complex permittivity, (c) dielectric loss tangent. (d) Real and (e) imaginary part of complex permeability, (f) magnetic loss tangent.

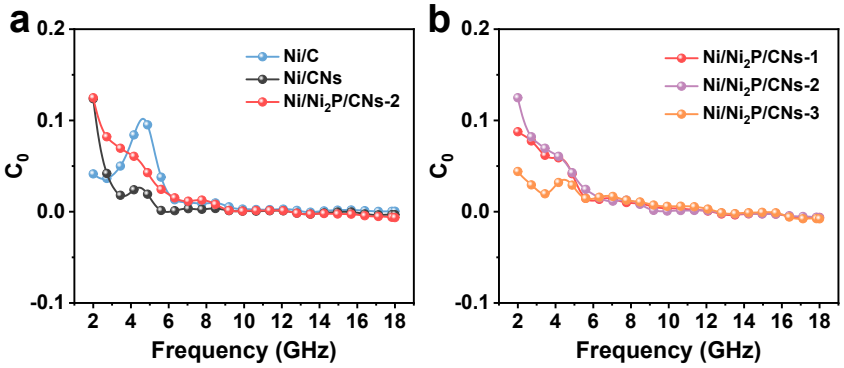

Fig. S13 Eddy current loss of Ni/C, Ni/CNs, and Ni/Ni_2P/CNs-x.

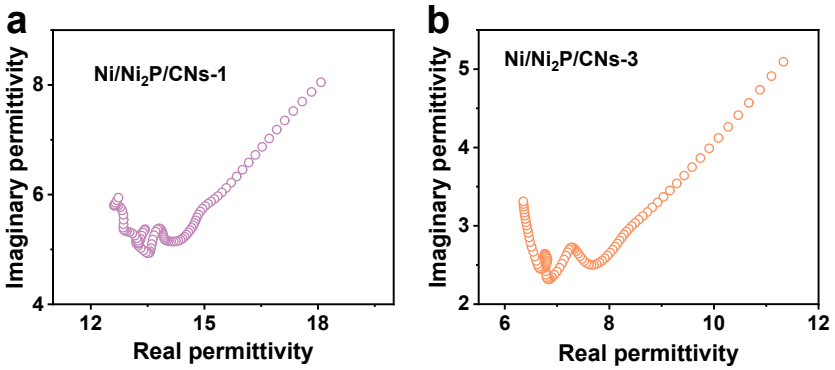

Fig. S14 The ε′ versus ε″ curves of (a) Ni/Ni_2P/CNs-1 and (b) Ni/Ni_2P/CNs-3.

References:

1 W. Hou, B. Wang, S. Li, F. Huang, H. Yang and H. Zhang, *J. Mater. Chem. A*, 2023, DOI: 10.1039/d3ta03740a.

2 N. Zhai, J. Luo, P. Shu, J. Mei, X. Li and W. Yan, *Nano Res.*, 2023, **16**, 10698-10706.

3 B. Li, Z. Ma, J. Xu, X. Zhang, Y. Chen and C. Zhu, *Small*, 2023, **19**, 2207197.

4 B. Li, Z. Ma, X. Zhang, J. Xu, Y. Chen, X. Zhang and C. Zhu, *Small*, 2023, **19**, 2301226.

5 Y. Du, Z. Yan, W. You, Q. Men, G. Chen, X. Lv, Y. Wu, K. Luo, B. Zhao, J. Zhang and R. Che, *Adv. Funct. Mater.*, 2023, **33**, 2301449.

6 C. Wen, X. Li, R. Zhang, C. Xu, W. You, Z. Liu, B. Zhao and R. Che, *ACS Nano*, 2021, **16**, 1150-1159.

7 L. Rao, L. Wang, C. Yang, R. Zhang, J. Zhang, C. Liang and R. Che, *Adv. Funct. Mater.*, 2023, **33**, 2213258.

8 X. Han, Y. Huang, J. Wang, X. Du, L. Hu, T. Li and X. Sun, *Composites, Part B*, 2022, **239**, 109965.